Multichannel Bragg gratings in silicon waveguides with asymmetric sidewall modulation

Matthew W. Puckett,* Felipe Vallini, Andrew Grieco, and Yeshaiahu Fainman

Department of Electrical & Computer Engineering, University of California, San Diego, 9500 Gilman Dr., La Jolla, California 92023, USA

**Corresponding author: mwpucket@ucsd.edu*

Received November 24, 2014; revised December 14, 2014; accepted December 16, 2014; posted December 23, 2014 (Doc. ID 227165); published January 28, 2015

We demonstrate a new type of on-chip Bragg grating designed to possess multiple stopbands at predetermined wavelengths. By employing sidewall modulation to control the full width half-maximum and extinction ratio, and through the incorporation of multiple spatial frequencies into the gratings' periodicities, we show that Bragg reflection can be achieved at particular wavelengths of interest without compromising spectrally distinct characteristics. Multiple device geometries are theoretically studied using the finite-difference time-domain method, and the results these analyses yield are shown to be in good agreement with experimental data. We additionally demonstrate how such devices may be employed to fabricate so-called dual-mode Bragg gratings, which are capable of reflecting both TE- and TM-like modes at a single wavelength of operation.

OCIS codes: (050.0050) Diffraction and gratings; (130.7408) Wavelength filtering devices; (230.1950) Diffraction gratings; (070.7345) Wave propagation.

http://dx.doi.org/10.1364/OL.40.000379

In the rapidly growing field of integrated photonics for optical communications, one critical device component is the now well-established Bragg grating [1]. By periodically modulating a waveguide's effective index, predetermined spectral properties may be incorporated into such optical devices as modulators, wave mixers, optical switches, and wavelength division multiplexers [2–4]. Resonant and interferometric structures such as ring resonators and Mach–Zehnder interferometers are also commonly employed in many wavelength-sensitive applications [5,6], but in an integrated silicon platform, waveguide gratings formed through sidewall modulation exhibit improved performance in terms of simultaneous control of the full width half-maximum (FWHM) and extinction ratio.

In optical signal processing, when it becomes necessary to simultaneously reflect multiple wavelengths, two or more spatially distinct gratings are often employed [7]. In the context of many processes, however, this can lead to phase mismatch, pulse deformation, or complications regarding the co-alignment of input wavelengths with resonant device wavelengths. Here we introduce a new Bragg grating configuration achieved through asymmetric sidewall modulation of a silicon waveguide, which aims to simultaneously reflect multiple wavelengths within a spatially overlapping region. Although we only consider the case of two reflected wavelengths in this work, we emphasize that asymmetric gratings may be scaled to possess more than two stopbands without increasing the total device length by employing core or cladding modulation [8], which leads to a significantly reduced device footprint in comparison to cascaded conventional gratings.

The reflection spectrum of a Bragg grating may be obtained by taking the spatial Fourier transform of a periodic perturbation to a waveguide [9–11]. This effect has been exploited in the literature to design such exotic diffractive optical components as multichannel mirrors and dispersion compensated reflectors [12–16]. However, these efforts have been limited largely to the regime of optical fibers in which distinct spatial frequency components may be easily superimposed over one another through UV exposure. Although there have been on-chip demonstrations of multichannel reflection in Bragg gratings [17], the modulation architecture employed, namely high aspect-ratio sidewall modulation, inevitably gives rise to scattering losses due to increased modal overlap with etched surfaces. Weak sidewall modulation allows these losses to approach those of the unperturbed waveguide [18] and also allows the stopband depth to be more precisely controlled. In this work we theoretically analyze, fabricate, and experimentally characterize several sidewall-modulated multichannel Bragg gratings made through a CMOS-compatible fabrication process. We also demonstrate that such gratings may be used to reflect multiple waveguide modes, particularly the lowest order TE- and TM-like modes, at a common wavelength of operation, an important functionality in emerging technologies [19].

Our modulation scheme is shown in Fig. 1(a), and it includes periodic perturbations to both of the two sidewalls of a silicon waveguide. The modulation depths and periods are allowed to vary independently for each sidewall, and the difference in spatial frequency between the

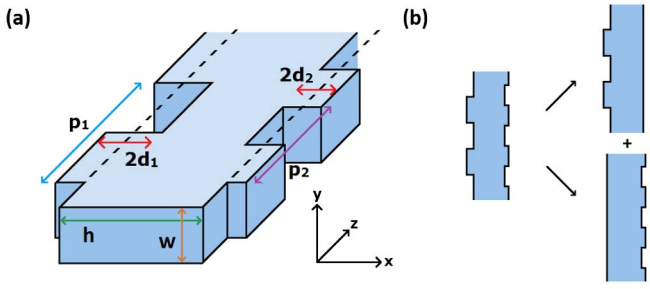

Fig. 1. (a) Schematic illustrating the layout of the demonstrated device consisting of a silicon waveguide including independent perturbations to its two sidewalls. (b) Illustration showing the conceptual treatment of the device in which the total grating is decomposed into two constituent sub-gratings.

two perturbations is what allows for the existence of two spectrally independent stopbands. The theoretical treatment of the grating is surprisingly straightforward. The spectral properties of the multichannel grating may be considered to be a superposition of the spectral properties of two more basic gratings, which only contain modulation along one sidewall, as shown in Fig. 1(b). This treatment is valid as long as, for a single mode, the stopbands corresponding to the two sub-gratings do not significantly overlap.

The coupling coefficient for an arbitrary periodic perturbation to a waveguide may be calculated in a number of ways. Here, we define it as [20]

$$\kappa = \frac{k_0}{2n_{\text{eff}}} \frac{\iint \Delta n^2(x,y) E^2(x,y) \mathrm{d}x\mathrm{d}y}{\int E^2(x,y)\mathrm{d}x\mathrm{d}y}, \tag{1}$$

where Δn is the spatially variant change in the refractive index introduced by the grating. Although it is not immediately clear whether this expression remains accurate for gratings containing multiple spatial frequencies, our following results suggest that the superposition technique employed here is largely valid. A more thorough treatment of the coupled mode theory of asymmetric gratings is very worthwhile, and may be considered in subsequent work.

For the grating under consideration, we choose a width of 400 nm, a modulation depth of ±20 nm for each sidewall, and a waveguide height of 220 nm. For this geometry the value of κ for each sub-grating evaluates to $2.32(10^4)$ and $5.64(10^3)$ m^{-1} for the TE- and TM-like modes, respectively. In order to predict how these gratings should behave, we chose to solve the wave propagation exactly using the finite-difference time-domain (FDTD) tool Lumerical [21]. Assuming a length of 40 μm, Fig. 2 shows the transmission spectra of the TE- and TM-like modes through several different asymmetric gratings. Multiple stopbands are clearly visible in each case, and are offset in general by

$$\lambda_1 - \lambda_2 = 2(n_1 p_1 - n_2 p_2), \tag{2}$$

where n_1 and n_2 are the effective indices for the unperturbed waveguide at λ_1 and λ_2, respectively, and p_1 and p_2 are the modulation periods. The stopbands corresponding to the TE- and TM-like modes are shown in Fig. 2 to have dissimilar depths and widths, and this is a direct result of the smaller overlap of the TM-like mode with the waveguide sidewalls, which yield a decreased value of the coupling coefficient. The FWHM of a Bragg grating's stopband may be approximately calculated as [20]

$$\Delta\lambda = \frac{\lambda^2}{n_g L}\sqrt{1 + \left(\frac{\kappa L}{\pi}\right)^2}, \tag{3}$$

where n_g is the group index of the guided mode and L is the length of the grating. It then follows naturally that reduced values of κ for a given grating length will lead to stopbands that are both narrower and shallower. The difference in behavior between the two modes supported by our chosen waveguide dimensions may easily be compensated for in subsequent iterations by selectively increasing the sidewall modulation depth for the TM-like modes.

Based on our FDTD results, we fabricated and experimentally characterized Bragg gratings possessing the properties defined in our models. To fabricate our devices, we began with an SOI wafer consisting of a 220 nm thick device layer and a 3 μm thick buried oxide layer. We spun the electron-beam resist hydrogen silsesquioxane onto these wafers and then wrote our waveguide patterns, including several different 200 μm long gratings, into the resist through electron-beam lithography. Next, we removed the unexposed resist by developing the wafer in a solution of tetramethylammonium hydroxide. We then etched away the unwanted silicon device layer through reactive ion etching and deposited a 1.3 μm thick silicon dioxide cladding layer through plasma-enhanced chemical vapor deposition. A scanning electron microscope (SEM) micrograph of one of our gratings is shown in Fig. 3, prior to the deposition step. The micrograph shows an apparent smoothing of the sidewall modulation in comparison to the FDTD model, as well as a slight decrease from the target modulation depth of ±20 nm.

To characterize our multichannel gratings, we coupled horizontally and vertically polarized laser light, tunable from 1465 to 1570 nm, into the waveguides using a lensed

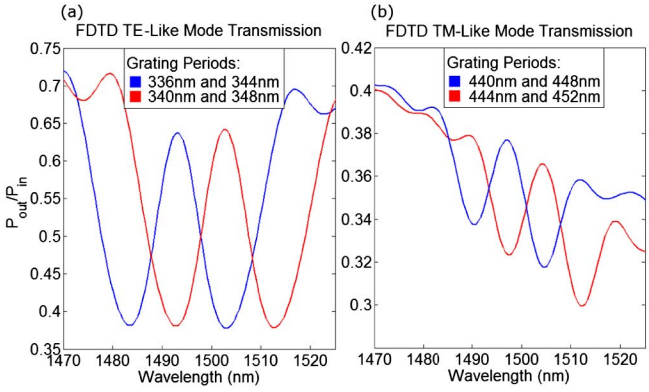

Fig. 2. FDTD-generated transmission spectra through an asymmetric grating assuming (a) TE-polarized light and grating periods of 336 and 344 nm (blue) and 340 and 348 nm (red), and (b) TM-polarized light and grating periods of 440 and 448 nm (blue) and 444 and 452 nm (red).

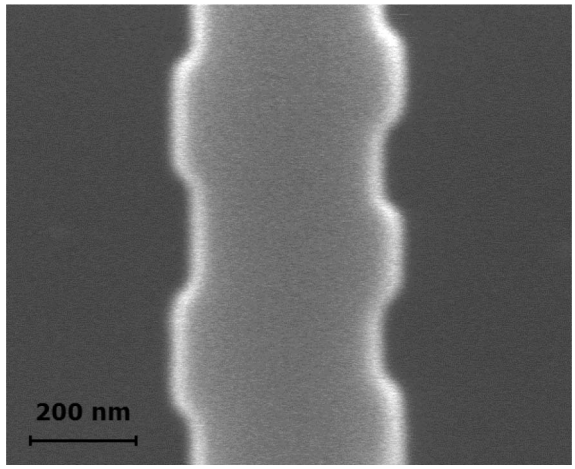

Fig. 3. SEM micrograph showing the top view of one of the fabricated asymmetric gratings.

tapered fiber. We then collected the light transmitted through the devices using a metallic objective and an optical setup consisting of two 4 F systems. This measurement setup has been used in previous DBR characterizations [22]. Five gratings were fabricated for each of the considered cases and were seen to behave almost identically, suggesting very high repeatability. The losses measured from the input optical fiber to the optical power meter were approximately 30 and 20 dB for the TE- and TM-like modes, respectively. Comparable values were observed for straight waveguides, suggesting that the gratings themselves did not exhibit appreciable losses off-band.

The obtained transmission spectra shown in Fig. 4 exhibit two distinct stopbands for each individual grating, and the stopbands are displaced from one another by an amount in agreement with Eq. (2). The experimental FWHM of the stopbands were approximately 8 nm for the TE-like mode and 2 nm for the TM-like mode, in comparison to respective FDTD values of approximately 12 and 8 nm. Referring again to Eq. (3) we may conclude that the coupling coefficients of the fabricated gratings are somewhat smaller than the corresponding FDTD values.

The fluctuations exhibited by the experimental transmission spectra are likely the result of Fabry–Perot effects arising from reflections at the waveguide end facets and at the interfaces between the straight waveguide sections and the gratings. These fluctuations may be reduced in the future by incorporating adiabatic tapers into our devices at each interface. Additionally, the downward tilt present in the FDTD transmission spectrum of the TM-like mode is not exhibited by our fabricated devices. This is likely due to the reduced experimental coupling coefficient, which consequently lessens the reflection at the interface between the waveguide and the grating.

For our dual-mode gratings we characterized the transmission of both TE- and TM-polarized light through a single device. Our results, shown in Fig. 5, verify that both polarization states are reflected at a wavelength of approximately 1477 nm for grating periods of 436 and 336 nm. By making fine adjustments to the period

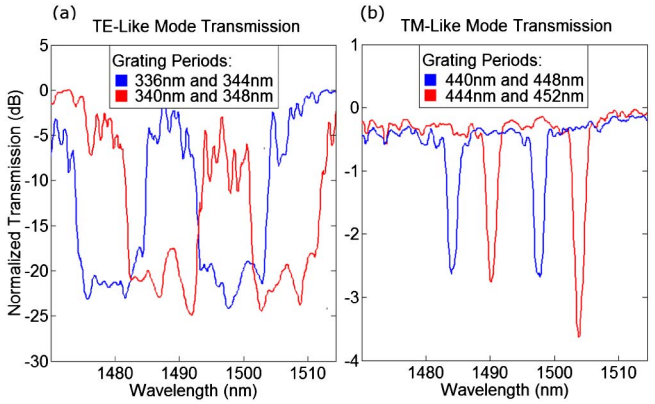

Fig. 4. Experimental transmission spectra through an asymmetric grating assuming (a) TE-polarized light with grating periods of 336 and 344 nm (blue) and 340 and 348 nm (red), and (b) TM-polarized light with grating periods of 440 and 448 nm (blue) and 444 and 452 nm (red).

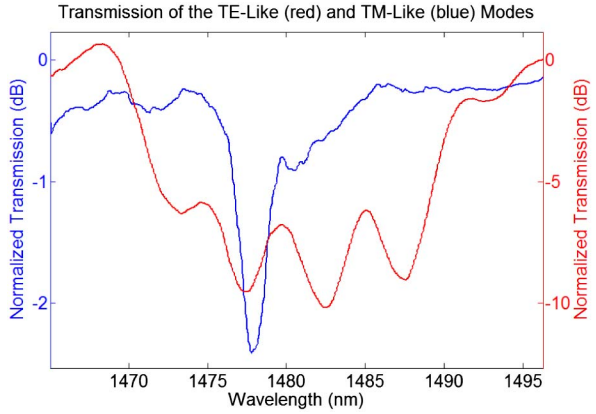

Fig. 5. Dual-mode transmission spectra showing the simultaneous reflection of the TE- and TM-like mode at a wavelength of approximately 1477 nm for asymmetric grating periods of 436 and 336 nm.

and modulation depth of each sub-grating, it is straightforward to more exactly align the stopbands of the two modes with each other and to achieve more comparable extinction ratios.

In conclusion, we have shown that asymmetric gratings may be used (a) to generate more than one stopband for a single guided mode of a waveguide and (b) to reflect two different modes at the same wavelength, allowing for the design of a polarization insensitive mirror. These results have significant implications for the field of optical signal processing, and may eventually be applied to such advanced devices as supercontinuum reflectors, multichannel add–drop filters [23], and mode-sensitive optical circuits.

This work was supported by the Defense Advanced Research Projects Agency (DARPA), the National Science Foundation (NSF), the NSF ERC CIAN, the Office of Naval Research (ONR), the Multidisciplinary University Research Initiative (MURI), and the Cymer Corporation. Sample fabrication was performed at the UCSD Nano3 cleanroom facility. Sample characterization was performed at the Chip-Scale Photonic Testing Facility, a collaboration between UCSD and Agilent technologies, which we gratefully acknowledge.

References

1. A. Yariv and P. Yeh, *Photonics: Optical Electronics in Modern Communications* (Oxford, 2006).
2. M. Puckett, J. Smalley, M. Abashin, A. Grieco, and Y. Fainman, Opt. Lett. **39**, 1693 (2014).
3. G. Klemens, C. Chen, and Y. Fainman, Opt. Express **13**, 9388 (2005).
4. P. Sansonetti, C. Sinet, L. Gasca, L. Martineau, S. Lacroix, X. Daxhelet, and F. Gonthier, Electron. Lett. **33**, 803 (1997).
5. D. Thomson, F. Gardes, Y. Hu, G. Mashanovich, M. Fournier, P. Grosse, J. Fedeli, and G. Reed, Opt. Express **19**, 11507 (2011).
6. G. Li, X. Zheng, J. Yao, H. Thacker, I. Shubin, Y. Luo, K. Raj, J. Cunningham, and A. Krishnamoorthy, Opt. Express **19**, 20435 (2011).
7. C. Giles, J. Lightwave Technol. **15**, 1391 (1997).
8. D. Tan, K. Ikeda, and Y. Fainman, Opt. Lett. **34**, 1357 (2009).
9. H. Li, Y. Sheng, Y. Li, and J. Rothenberg, J. Lightwave Technol. **21**, 2074 (2003).

10. M. Ibsen, M. Durkin, J. Cole, and R. Laming, IEEE Photon. Technol. Lett. **10**, 842 (1998).
11. F. Ouellette, P. Krug, T. Stephens, G. Dhosi, and B. Eggleton, Electron. Lett. **31**, 899 (1995).
12. A. Srinivasan, Y. Shih, J. Campbell, B. Streetman, J. Bean, and L. Peticolas, in *Proceedings of IEE/LEOS Summer Topical Meetings: Integrated Optoelectronics* (IEEE, 1994).
13. D. Lovering, G. Fino, C. Simonneau, R. Kuszelewicz, R. Azoulay, and J. Levenson, Electron. Lett. **32**, 1782 (1996).
14. P. Perez-Millan, M. Andres, and P. Hedekvist, J. Lightwave Technol. **24**, 329 (2006).
15. D. Tan, K. Ikeda, R. Saperstein, B. Slutsky, and Y. Fainman, Opt. Lett. **33**, 3013 (2008).
16. D. Tan, K. Ikeda, and Y. Fainman, Appl. Phys. Lett. **95**, 141109 (2009).
17. A. Hayat and M. Orenstein, Opt. Lett. **32**, 2864 (2007).
18. A. Grieco, B. Slutsky, and Y. Fainman, Appl. Phys. B **114**, 467 (2014).
19. L. Luo, N. Ophir, C. Chen, L. Gabrielli, C. Poitras, K. Bergmen, and M. Lipson, Nat. Commun. **5**, 3069 (2014).
20. H. Kogelnik, Integr. Opt. **7**, 13 (1975).
21. www.lumerical.com/tcad-products/fdtd.
22. A. Grieco, B. Slutsky, D. Tan, S. Zamek, M. Nezhad, and Y. Fainman, J. Lightwave Technol. **30**, 2352 (2012).
23. K. Ikeda, M. Nezhad, and Y. Fainman, Appl. Phys. Lett. **92**, 201111 (2008).